H. Truong, A. Marouf, J. B. Vos, A. Gehri, M. Braza, Y. Hoarau (2023), "Numerical investigation of Active Flow Control using Zero Net Mass Flux jets around a high-lift morphing cambered wing-flap system", International Journal of Numerical Methods for Heat & Fluid Flow.
https://doi.org/10.1108/HFF-09-2022-0558

Numerical investigation of Active Flow Control using Zero Net Mass Flux jets around a high-lift morphing cambered wing-flap system

H. Truong*[1], A. Marouf[1], J. B. Vos[2], A. Gehri[2], M. Braza[3], and Y. Hoarau[1]

[1]ICUBE, University of Strasbourg, France

[2]CFS Engineering, EPFL Lausanne, Switzerland

[3]Institut de Mecanique des Fluides de Toulouse (IMFT), France

Abstract

Purpose - This study investigates the physical mechanisms of the use of Active Flow Control (AFC) for a high-lift wing-flap configuration.

Methodology - By means of high-fidelity numerical simulations, the flow dynamics around a high-lift wing-flap system at high Reynolds number (Re/c = 4.6 Million) is studied. Adapted turbulence models based on the URANS approach are used to capture the flow separation and the subsequent development of coherent structures. The present study focuses on the use of AFC using a synthetic jet known as Zero Net Mass Flux (ZNMF) using the blowing-suction approach. Different parameters (geometry, frequency and velocity) of a ZNMF placed at the cambered flap's chord are optimized in order to obtain the most efficient parameter settings to suppress the flow separation.

Findings - A synthetic jet with the optimal shape and orientation enforces the flow re-attachment on the wing-flap surface. This leads to an improvement of the aerodynamic performance of the system. The wake thickness was reduced by 30%, and an increase of 17.6% in lift-to-drag ratio was obtained. Concerning the ZNMF location, they should be installed upstream of the separation point to achieve the best performance.

Originality - The effectiveness of ZNMF devices integrated on a high-lift wing-flap configuration was studied in real flight conditions at high Reynolds number. A detailed analysis of the wake dynamics explains how AFC forces the re-attachment of the boundary layer and attenuates the predominant wake instabilities up to $-20\,\mathrm{dB}$.

Keywords

Active flow control; Zero-Net-Mass-Flux; High lift system; CFD; Aerodynamics; Turbulence

*Corresponding Author: dh.truong@unistra.fr

NOMENCLATURE

C_p	=	pressure coefficient
CD	=	Drag coefficient
CL	=	Lift coefficient
c	=	chord
d	=	jet diameter
dt	=	time step
f_{jet}	=	jet frequency
F^+	=	jet dimensionless frequency
C_μ	=	blowing momentum coefficient
V_{jet}	=	jet velocity magnitude
ρ	=	air density
Re	=	Reynolds number
U_∞	=	streamflow velocity

1 INTRODUCTION

One of the main concerns of the aviation industry in the modern world is to lower its negative impacts on the environment (carbon dioxide emission, aircraft noise, fossil fuel burn, etc.). To meet this challenge, a variety of active flow control (AFC) techniques have been developed to improve the aerodynamic performance of airfoils and wings by controlling the flow separation. Among them, synthetic jet actuation (SJA), also known as zero-net-mass-flux (ZNMF), have been worldwide intensively investigated due to its effectiveness and simple implementation. These actuators do not require a piping for pressurized air source, yet create non-zero-net momentum flux via periodic suction and injection of fluid through an orifice. The efficiency of ZNMF actuators depends on various parameters of which two key ones are the dimensionless frequency of the jet $F^+ = f_{jet}c/U_\infty$ and the ratio of the actuator velocity to the free-stream velocity V_{jet}/U_∞ (or the blowing momentum coefficient $C_\mu = 2dV_{jet}^2/cU_\infty^2$).

Seifert and Pack (1999) was one of the first to conduct experiments to study the effectiveness of synthetic jets at high Reynolds numbers (around 10^7). The active flow control was applied for a NACA0015 airfoil without flap as well as a NACA0015 airfoil equipped with a 30% chord trailing-edge flap deflected $20°$. The study demonstrated the effectiveness of oscillatory blowing-suction for flow separation control regardless of the Reynolds number. McCormick (2000) investigated experimentally the use of a synthetic jet located at 4% chord from the leading edge for control of the flow separation at $Re = 5 \times 10^5$. The synthetic jet with an oscillation frequency ($F^+ = 1.3$) and jet momentum coefficient ($C_\mu = 0.5\%$) can increase the maximum lift

coefficient by 25% and mitigate the stall angle by 6°. Tuck and Soria (2004) conducted experiments of a flow over a NACA0015 airfoil ($Re = 1.54 - 3.08 \times 10^4$) with a ZNMF jet located at the leading edge. An increase of 46% in the maximum lift coefficient was obtained for the jet conditions of $F^+ = 1.3$ and $C_\mu = 0.14\%$. Tang *et al.* (2014) studied the effects of synthetic jet arrays placed at 23% and 43% of the chord on the aerodynamic performance of an LS(1)-0421MOD airfoil at a Reynolds number $Re = 1.2 \times 10^5$. The synthetic jets permitted to increase the lift by 27% and to reduce the drag by 19%.

The influence of synthetic jets has also been investigated by many numerical studies on different airfoils. Donovan *et al.* (1998) employed a URANS approach to study the application of unsteady jets on a NACA0012 airfoil at high Reynolds number $Re = 8.5 \times 10^6$. For a non-dimensional frequency $F^+ \approx 1$, a synthetic jet placed at 1.5% chord with an inclination angle $\alpha = 22^\circ$ could improve the lift by 27%. They also found that the lift was inversely proportional to the blowing momentum coefficient C_μ. By employing an unstructured-grid LES method, You and Moin (2008) analyzed the flow separation over a NACA0015 with synthetic jet control at a Reynolds number of 8.96×10^5. The study confirmed the experiments conducted by Gilarranz *et al.* (2005) where the airfoil was installed in a wind tunnel with a synthetic jet at 12% of the chord. A 70% increase in lift coefficient was obtained with a jet of which the momentum coefficient was 1.23%. Kim and Kim (2009) studied numerically the benefits of single and multiple synthetic jets on a NACA23012 airfoil by solving the URANS equations at $Re = 2.19 \times 10^6$. In the case of multiple synthetic jets, several jets were arranged side by side to overcome the limits of the jet peak velocity. The study showed that the jets operating at a frequency of $F^+ = 1$ should be placed at the separation point to reach the maximum lift, and the effectiveness of the jet was proportional to the jet momentum.

An automatic optimization of the parameters and locations of flow control devices requires enormous computational resources due to the need of a large number of high accuracy unsteady numerical simulations. To the best of our knowledge, there are only a few studies acquiring optimal parameters of synthetic jets by employing optimization algorithms. Duvigneau and Visonneau (2006) examined the effects of a synthetic jet located at 12% chord from the leading edge of a NACA0015 airfoil. They used the URANS approach to simulate the flow at $Re = 8.6 \times 10^5$ over the airfoil with an angle of attack varying from 12° to 24°. The solver was then coupled with an optimization procedure to find the optimal parameters of the jet. The synthetic jet reached its optimal performance under the conditions of a dimensionless velocity $V_{jet}/U_\infty = 1.72$, a frequency $F^+ = 0.748$ and an jet angle with respect to the wall $\alpha = 25^\circ$. Montazer *et al.* (2016) determined the optimal parameters of a synthetic jet for flow control around the NACA0015 airfoil at the stall angle 13° and the post stall angle 16°. The Navier–Stokes equations for an incompressible two-dimensional flow were solved by a RANS model at $Re = 8.96 \times 10^5$. An optimization method, called Response Surface Methodology (RSM), was then employed to maximize the lift-drag ratio where the optimization parameters were the jet location, the jet frequency and the jet size. According to their study, as the angle of attack increased, the size of the synthetic jet and the frequency should decrease to obtain the optimal performance. Under this circumstance, the optimum synthetic

jet location was moving toward the leading edge to delay the flow separation. The synthetic jet was shown to be the most effective at the post-stall angle with an 66% improvement of the lift-drag ratio.

Although the benefits of employing ZNMF devices for relatively simple airfoils have been pointed out by previous studies, the effectiveness of integrating ZNMF devices into 3D multi-element high-lift systems remains an open question. Mechanical high-lift devices (e.g. slats and flaps) have been developed to ensure sufficient performance for take-off and landing phases. The design of these systems have almost reached their limits such that they are as simple as possible while generate enough lift during operational conditions. Further optimisation of a high-lift system is very costly and the results do not match the amount of effort expended on the research. On the other hand, modern flow control methodologies are the most promising for high-lift applications. Among recent European research projects funded under the EU funded Horizon 2020 program, the SMS project (Smart Morphing and Sensing for aeronautical configurations[1]) focused on the disruptive wing design based on bio-inspired electroactive morphing. The project demonstrated a considerable aerodynamic performance increase for an Airbus A320 morphing prototype in different flight phases: low subsonic (take-off and landing) as well as transonic (cruise). An association of high-deformation cambering and combined with trailing edge vibration, in the context of the so-called "hybrid electroactive morphing" (Marouf *et al.*, 2019), produced a further increase in aerodynamic performance. In previous studies Marouf *et al.* (2021, 2022), we used a hybrid model (DDES-SA) to analyze the interaction between a wing and flap shear-layers in a 3D configuration using a small span wing. It was found that the use of a ZNMF device caused the flow to reattach and delay the merging of the shear-layers. The studies also utilized a larger span with URANS modeling to study different locations of real jets, while taking into account limitations of the mass flux produced by existing piezo-actuators. The results indicated that steady blowing with different jet intensities led to important reattachment, and that the distance between the jets resulted in the formation of two counter-rotating vortices that interacted with each other and with the injected jet. The unsteadiness of the flow strengthened this interaction, causing the separation to travel upstream. The study also found that the periodicity of the jet blowing-suction helped this process, and that the ZNMF devices should be installed upstream of the flow separation and kept close to the separation to avoid jet momentum dissipation. It was also noted that ZNMF jets immersed within a flow separation lose their effectiveness.

This paper is concerned with numerical studies of ZNMF devices on the high-lift wing-flap system of the Large-Scale (LS) prototype of the SMS project. The velocity, frequency, location and geometry of the ZNMF jet are examined using 2D high-fidelity numerical simulations. The outcome of this study will be used in the CleanSky 2 project AFC4TR (Active Flow Control for a Tilt Rotor) No 886718 [2] that started in September 2020. The overall objective of the AFC4TR project is to investigate the use of Active Flow Control using ZNMF devices on the Leonardo Next-Generation Civil Tiltrotor (NextGenCTR or NGCTR) aircraft.

[1] www.smartwing.org/SMS/EU
[2] www.afc4tr.eu

2 NUMERICAL METHODS

2.1 NSMB solver

The CFD simulations were carried out using the Navier Stokes Multi Block solver NSMB developed in a consortium composed of different universities and industries. NSMB is a cell-centered finite volume solver using multi block structured grids. Both the patch grid and chimera method are available to simplify the mesh generation for complex geometries. The solver includes a large variety of turbulence models that are standard in the aeronautical industry. For unsteady CFD simulations Hybrid RANS-LES models are available as well as the $k - \omega$ Organized Eddy Simulation model which were used for 2D and 3D simulations. Furthermore, morphing wings strategies have been implemented in the solver and have been proven. For more details, we refer to (Hoarau *et al.*, 2016; Marouf *et al.*, 2019).

2.2 Computational setup for two dimensional simulations

The 2D numerical studies discussed in this section were made with the inflow conditions of $U_\infty = 69.35\,\mathrm{m\,s^{-1}}$ ($Ma = 0.2$) and $Re = 4.66 \times 10^6$. The high lift wing-flap system is studied with the flap detached from the airfoil. The deflected angle is around 10° corresponding to the take-off position for an A320 wing. The resulting total chord of the airfoil and the flap in this case is about $2.72\,\mathrm{m}$. The computational domain is extended up to 20 times the chord of the wing-flap system with far-field condition imposed at the boundaries as shown in Fig. 1. For a simple airfoil at small angle of attack, the flow separation has not occurred yet and the influence of synthetic jets is usually insignificant Donovan *et al.* (1998). However, for the high-lift system studied here, the wing was set with a small angle of attack at 4°, but the morphing with the cambering flap up to 10% of its chord induced a detachment of the boundary layer near the trailing edge of the flap. These conditions permit to study the possibility of ZNMF devices to control the flow separation leading to a re-attachment of the flow.

To simplify the mesh generation for this configuration both the sliding mesh approach as well as the Chimera overlapping technique were employed. Indeed, these techniques allow to create one structured multi block grid for a single configuration, and obtain the other configurations applying only rotations and displacements of partial grid elements (structured blocks) around the moving parts (the flap for example).

An O-grid topology with a specific arrangement of cells was used near solid surfaces (such as a wing or a whole aircraft) to resolve the flow near the viscous boundary layer. The first cell height in the direction perpendicular to the wall was chosen to maintain a low $y+$ value less than one, which is important for accurate turbulence modeling. The cell size in this direction typically increased by a factor of 1.2. The mesh in the regions near the trailing edges of the wing and flap were refined, as well as in areas where flow separation may occur. Special consideration was also given to refining the mesh in the vicinity of ZNMF devices.

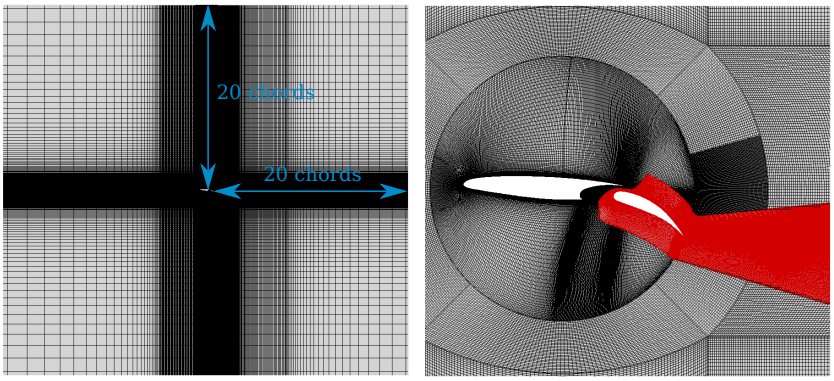

Figure 1: Left: Computational domain for 2D simulations with far-field boundary conditions. Right: Multi-blocks grid where the first grid (black) is the fluid domain including the wing and the second one (red) is around the flap.

2.3 Modeling of ZNMF jets

The ZNMF devices were inserted into the flap as an inclined rectangle (cf. Fig 2). On the boundary opposite to the jet a periodic blowing-suction boundary condition was imposed to simulate the ZNMF device. Several lengths (h), diameters (d) and inclination angles (β) of the devices were investigated (as shown in figure 2) and a trade-off of the best parameters will be presented. In order to isolate the effect of changing the ZNMF geometry, the frequency f as well as the mass flow q are fixed based on the ASPIC actuator presented previously. At an optimal frequency bandwidth around 200 Hz, the jet with a diameter $d = 1\,\mathrm{mm}$ can achieve a peak exit velocity V_0 of $150\,\mathrm{m\,s^{-1}}$. This results a maximum mass flow of the jet:

$$q_0^{ref} = V_0 \times d = 0.15\ \mathrm{m^2\,s^{-1}} \tag{1}$$

However, due to the inclined angle, the width w of the ZNMF is not the same as the output diameter d. Consequently, the maximum mass flow of the ZNMF in our model is calculated by:

$$q_0 = V_0 \times w = V_0 \times d \times sin(\beta) = 0.15\ \mathrm{m^2\,s^{-1}} \tag{2}$$

Since different diameters are studied, the jet velocity needs to be adjusted to get the same mass flow for all cases by using Eqn 2. In addition, the height h of the cavity is also modified to keep the aspect ratio unchanged. Consequently, there are in total eight configurations that are investigated where the different parameters are summarized in table 1. From a modeling point of view, there are commonly two proposed methods for modeling the jet velocity. The first method consists of imposing directly the velocity while the second one simulates the movement of the ZNMF membrane located at the bottom of the cavity. As mentioned above, the former method was chosen in our model for its simplicity and it captures correctly the physics of ZNMF devices.

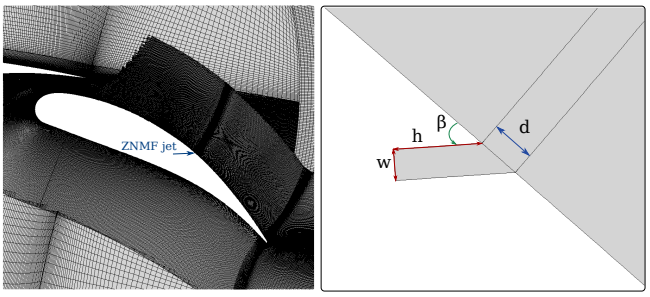

Figure 2: Left: ZNMF jet is located at 60% chord of the cambered flap for separation flow control. Right: the geometrical definition of the ZNMF device modeled by an inclined rectangle.

Configuration	Diameter (mm)	Height (mm)	Inclined angle (degree)	Dimensionless velocity V_{jet}/U_∞	Mass flow ($\mathrm{m^2\,s^{-1}}$)	Dimensionless frequency F^+
1	1	2	30	4.326	0.150	7.844
2	1	2	45	3.057		
3	3	6	15	2.768		
4	3	6	30	1.442		
5	3	6	45	1.024		
6	5	10	15	1.658		
7	5	10	30	0.865		
8	5	10	45	0.606		

Table 1: Geometrical and physical parameters that are used for the study of the influence of ZNMF geometry on the aerodynamic performance of the morphing high-lift system. The parameters are adjusted in each case to ensure that the mass flow and the jet frequency are the same for all cases.

3 RESULTS AND DISCUSSION

3.1 Mesh convergence study

A grid sensitivity study for the 2D case was performed using three different grids (coarse, medium and fine) of which the number of cells are $186\ 000, 743\ 000$ and 3 million, respectively. From the comparisons of the computed forces in Fig. 3, the result obtained for the medium and fine grids are close enough to establish that the grid independence is reached. The differences of the averaged lift and drag between these two grids (cf. table 2) are 0.47% and 4.28%, respectively. Since the computational cost increases rapidly with the mesh refinement level and because a large number of unsteady simulations will be performed in the optimization procedure, the medium grid is chosen for the next studies.

	C_L	C_D
Coarse	2.464	0.0606
Medium	2.578	0.0559
Fine	2.566	0.0584

Table 2: Time averaged drag and lift coefficients on the three grids: coarse, medium and fine.

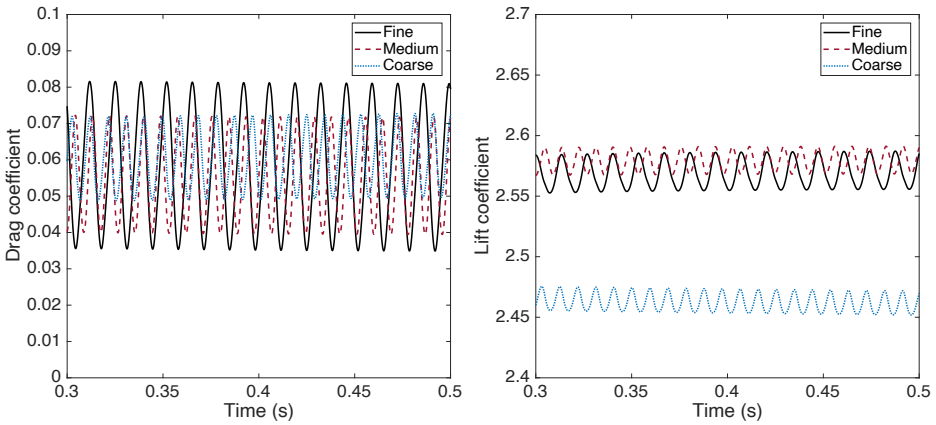

Figure 3: Drag and lift coefficients solved by the three grids: coarse (blue), medium (red) and fine (black).

3.2 Effects of the ZNMF geometry

In order to quantify the effect of the use of ZNMF devices on the aerodynamic performance of the high-lift system, time-averaged lift and drag coefficients are calculated for the baseline configuration without flow control and for the eight configurations using ZNMF devices. All the simulations were run for at least 60000 time steps and the results of the last 30000 time steps were averaged to get the force coefficients. Fig 4 presents the variation of the aerodynamic forces with respect to the baseline. Overall, five of the eight configurations using ZNMF devices improve the aerodynamic performance characterized by a higher lift and a smaller drag. In addition, with the same mass flux, the ZNMF devices having a small diameter and a high peak velocity are more efficient in delaying the flow separation.

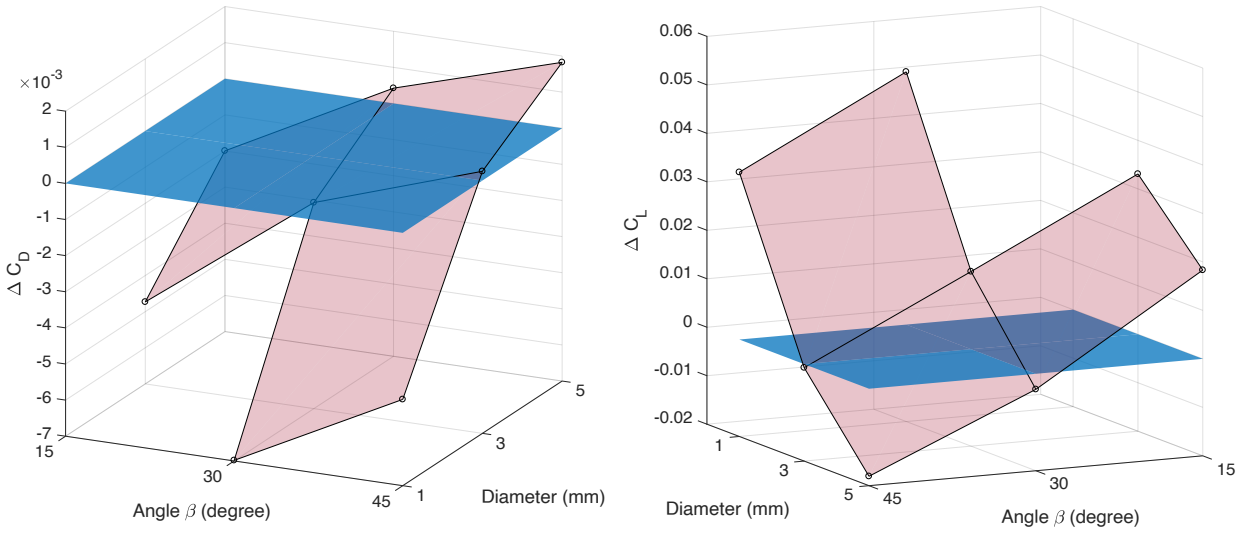

Figure 4: The effect of the ZNMF characterized by the variation of the drag (left) and the lift (right) coefficients with respect to the baseline (blue horizontal plan) without flow control.

In all simulations with ZNMF devices, the first configuration ($d = 1\,\mathrm{mm}, \beta = 30°$) appears to be the most optimal configuration while the eighth configuration ($d = 5\,\mathrm{mm}, \beta = 45°$) reduces the most the lift generation

Config. / Power ratio	1	2	3	4	5	6	7	8
$\frac{cU_\infty^3}{dV_{jet}^3}\frac{C_D - C_{D,baseline}}{C_{D,baseline}}$	-4.26	-7.97	-3.67	-7.11	3.93	-4.32	6.48	80.92

Table 3: The drag reduction power compared to the power supply for the jet in each case of the eight studied configurations.

of the system. The time history of the drag and lift coefficients of these two configurations along with the baseline configuration is presented in Fig. 5. The first configuration decreases not only the average drag by 13.26% but also the fluctuation, while the effect of the eighth configuration on the drag is negligible. On the other hand, the lift coefficient is enhanced with about 2.02% in the best case and reduced about 0.7% in the worst case. These results leads to an improvement of the lift-to-drag ratio up to 17.6% for the first configuration.

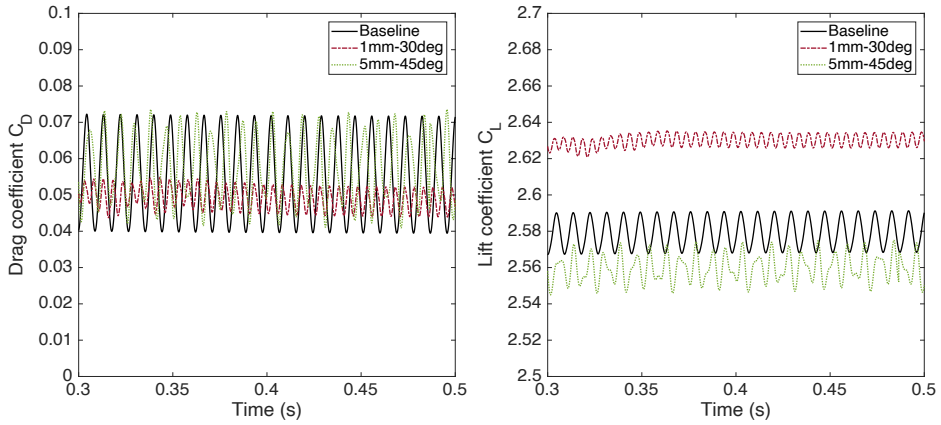

Figure 5: Time history of the drag coefficient (left) and the lift coefficient (right) calculated in the baseline (continuous black), the best case (dashed red) and the worst case (dot green).

Finally, it is interesting to evaluate the efficiency of the ZNMF jets from an energetic point of view. Table 3 presents the theoretical ratio between the power benefited from active flow control in term of drag reduction, defined as $1/2\rho c U_\infty^3 \Delta D$ with $\Delta D = (C_D - C_{D,baseline})/C_{D,baseline}$ (power per unit span) and the power supply needed for driving the ZNMF devices, defined as $1/2\rho d V_{jet}^3$ (power per unit span). Although the first configuration provides the best lift-to-drag ratio, the second configuration ($d = 1\,\mathrm{mm}, \beta = 45°$) and the fourth configuration ($d = 3\,\mathrm{mm}, \beta = 30°$) are more energetically efficient. With a smaller operating velocity, these configurations require less power consumption than the former. More specifically, the power saving by drag reduction obtained with the second configuration is almost 8 times larger than its power supply.

3.3 Flow analysis

To analyse in more detail the influence of the ZNMF jet on the flow characteristics, we first compare the boundary layer profiles of the non-dimensional longitudinal velocity component U_x/U_∞ in the normal direction of the bounding surface for the baseline, and for two jets having the best and the worst performance located in

the fully detached region on the flap as shown in Fig. 6. When there is no active flow control, a flow separation occurs inside the boundary layer that is subjected to the wall friction and is slowed down due to an adverse pressure gradient. The momentum of this flow is reduced, the energy in the boundary layer tends to zero and the flow is unable to overcome the pressure gradient. At some point, the viscous layer inside the boundary layer detaches from the surface of the wing and the streamlines near the wall separate from the flap surface. With the use of the ZNMF devices $1\,\mathrm{mm} - 30°$, the velocity profile shows that the reverse flow is effectively suppressed and the flow is reattached along the flap. This is explained by the fact that the blowing and suction of the synthetic jet enhance the momentum of the external flow to overcome the adverse pressure gradient. However, the ZNMF $5\,\mathrm{mm} - 45°$ with smaller blowing-suction velocity does not inject enough momentum into the external flow in order to delay the boundary separation. Obviously the amplitude of the jet plays an important role and controls the boundary layer profile.

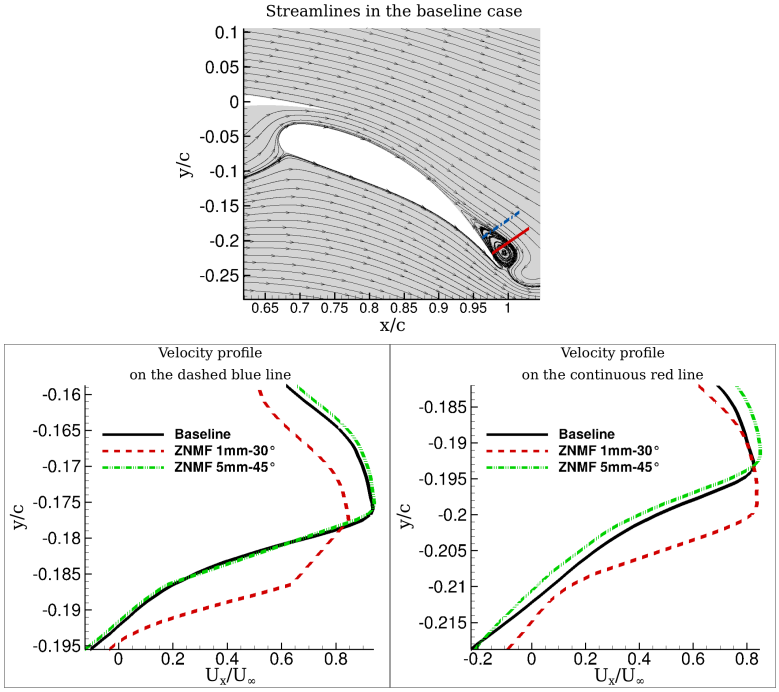

Figure 6: Top: Streamlines of the flow over the flap in the baseline case and the locations of the two lines (dashes blue and continuous red) of which the velocity profiles are investigated. Bottom: Comparison of non-dimensional longitudinal velocity field extracted on the two lines of the baseline (continuous black line), the best case (dashed red line) and the worst case (dashed dot green line).

Using ZNMF devices modify the flow near the trailing edge, and this has a significant influence on the wake of the airfoil. These modifications in turn affect the aerodynamic performance of the high-lift system. Thus, it is worthwhile to observe and discuss the airfoil-wake modifications, followed by a detailed analysis of the wake dynamics. Fig. 7 shows the time-averaged streamline around the wing-flap as well as the streamwise velocity (U_x) profile in the wake behind the high-lift system in the case of baseline and active flow control with the ZNMF $1\,\mathrm{mm} - 30°$ and the ZNMF $5\,\mathrm{mm} - 45°$. The time-averaged solution is calculated using a large number of snapshots saved each at a sampling rate of $1e^{-4}$ seconds. At a distance $x/c = 0.368$ (blue line)

and $x/c = 0.552$ (red line) behind the trailing edge, the axial velocity deficit reveals the wake formed behind the wing. The width of the wake is reduced with almost 30% for the case of flow control with the ZNMF $1\,\mathrm{mm} - 30°$ compared with the other two cases. This observation explains the reduction of the drag presented in the previous section.

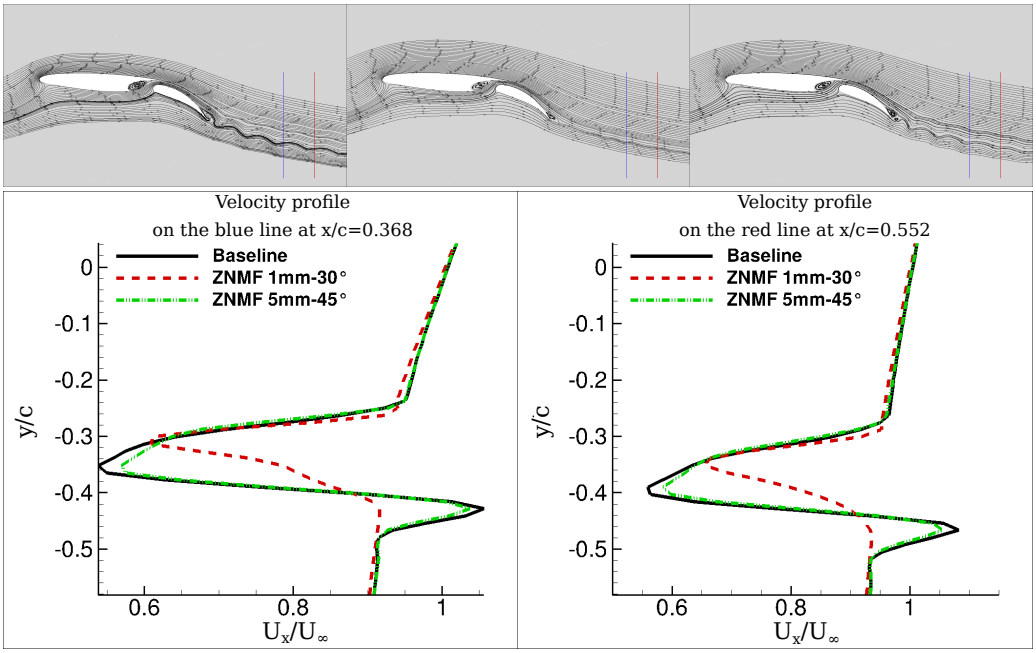

Figure 7: Axial component velocity (U_x) profile of the wake behind the high-lift system in the case of baseline and active flow control with the ZNMF $1\,\mathrm{mm} - 30°$ and the ZNMF $5\,\mathrm{mm} - 45°$. The velocity is plotted at $x/c = 0.368$ (blue line) and $x/c = 0.552$ (red line) behind the trailing edge. The width of the wake is reduced with almost 30% in the case of flow control with the ZNMF $1\,\mathrm{mm} - 30°$.

Furthermore, the time-averaged and the instantaneous vorticity fields (cf. Fig. 8) help to comprehend the wake modification due to the employment of the ZNMF devices. By design, a considerable vertical gap between the airfoil and the flap splits the shearing of these two elements in the wake. For the case without flow control, the flow separation happened at the trailing edge of the flap and makes the counterclockwise trailing edge vortex (TEV) roll up into the suction side and leads to the vortex shedding in the vicinity of the trailing edge. The non-linear interaction between the lower and upper shear layers of the airfoil and the flap generates unstable waves which are amplified when they propagate further downstream. When the ZNMF $1\,\mathrm{mm} - 30°$ is employed, the separation zone is reduced significantly. Thus, the circulation of the suction-side vortical structure is small and is not strong enough to influence the TEV. Consequently, the vortex sheet remains stable right behind the high-lift system and the Kelvin-Helmholtz instability is triggered further downstream compared to the baseline case. This leads to the attenuation of the wake formed afterwards. However, with the use of the ZNMF $5\,\mathrm{mm} - 45°$, the momentum injected into the flow is not enough to mitigate the flow separation and the shear-layer instabilities intensify again the unstable wake.

Next, the quantifiable impact of the ZNMF is investigated by looking at the Power Spectral Density (PSD) computed for signals measured at some monitor points in the wake by means of the Welch's weighted over-

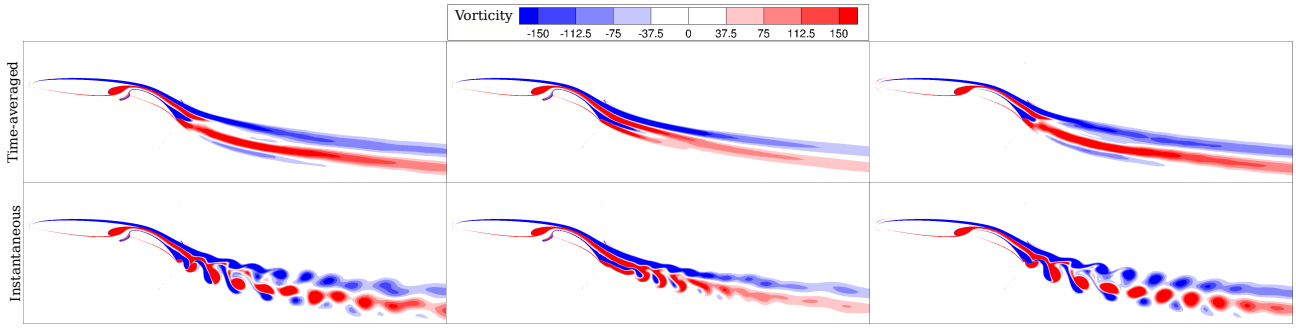

Figure 8: Time-averaged (top) and instantaneous (bottom) vorticity fields around the high-lift system in the case of baseline (left) and flow control with the ZNMF $1\,\mathrm{mm} - 30°$ (middle) and the ZNMF $5\,\mathrm{mm} - 45°$ (right).

lapped segment averaging estimator, using Hamming windows with 50% overlap and zero padding Welch (1967). This approach allows us to study the energy in a frequency domain and exhibits high energy modes related to the predominant instabilities created in the wake. Monitor points at different specific coordinates (cf. 9) for the baseline case and the controlled cases with the ZNMF $1\,\mathrm{mm} - 30°$ and the ZNMF $5\,\mathrm{mm} - 45°$ aiming to capture the motion of the low frequency instabilities of the wake and their modification due to the jets. A natural predominant frequency f_1 of the wake without flow control is estimated around $100\,\mathrm{Hz}$ and its corresponding harmonics represented by the black lines in Fig. 9. In the controlled case with the ZNMF $1\,\mathrm{mm} - 30°$, the PSD reveals a diminution of the wake amplitude with a decrease of the spectral energy between $10\,\mathrm{dB}$ to $20\,\mathrm{dB}$ related to the aerodynamic noise. Moreover, the ZNMF shifts the predominant frequency of the wake to a frequency $f_{jet} \approx 200\,\mathrm{Hz}$ which is the actuating frequency of the jet and it minimizes effectively higher harmonics. As expected, the ZNMF $5\,\mathrm{mm} - 45°$ has negligible impact on the spectral density of the wake as previously analyzed.

3.4 Effects of the ZNMF velocity and frequency

In this part, we are interested in studying the influence of the jet velocity and the frequency of the ZNMF device on the aerodynamic performance of the high-lift system. The time-averaged lift and drag coefficients are calculated while the dimensionless velocity V_{jet}/U_∞ is varied from 0.72 to 4.33 and the dimensionless frequency F^+ is varied from 1.96 to 11.77. The result is shown in Fig. 10. One can see that when the jet velocity V_{jet}/U_∞ is increased, the ZNMF energizes the boundary layer to delay the separation by injecting momentum to the external flow. This helps to increase the lift coefficient significantly and reduces the drag. However when the dimensionless velocity is higher than 2.88 ($V_{jet} = 200\,\mathrm{m\,s^{-1}}$), almost no further improvement can be observed. The sensitivity of the lift coefficient to the frequency variation is negligible while a higher blowing-suction frequency ($F^+ > 8$) appears to lower the drag. In terms of increased aerodynamic efficiency, the optimal parameters are a dimensionless velocity $V_{jet}/U_\infty > 2.88$ and dimensionless frequency $F^+ > 8$.

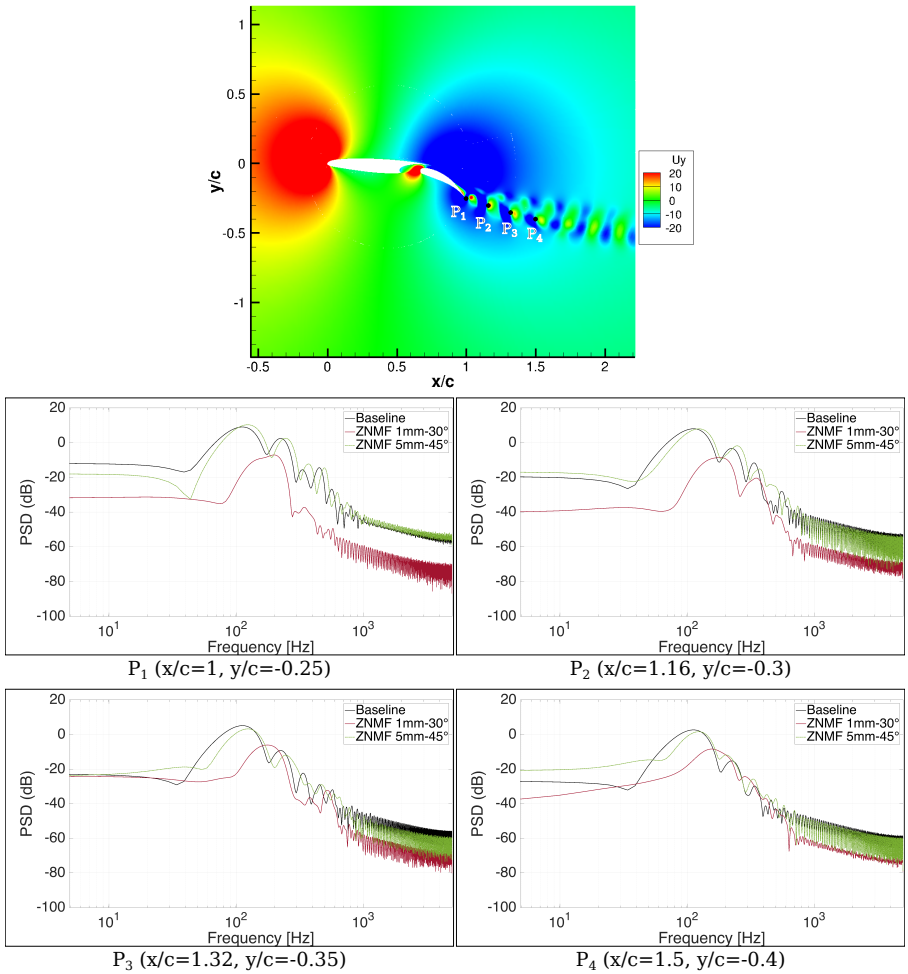

Figure 9: Power spectral density of the vertical velocity U_y for the baseline and the controlled cases at different monitor points P_1, P_2, P_3 and P_4 in the wake.

4 CONCLUSIONS AND PERSPECTIVES

High-fidelity numerical simulations have been carried out in the context of the European CleanSky2 project AFC4TR to study active flow control using ZNMF devices. Simulations were made on a 2D wing-flap configuration, for which morphing combined with cambering was used to deform the flap to find the optimal cambering shape. Using active flow control with ZNMF devices permitted to further improve the aerodynamic performance of the system by reattaching the flow to refrain the drag increase and to maintain the high lift force. The geometry of the ZNMF has been optimized to show that with a constant mass flux, one should favor a small ZNMF with high blowing-suction velocity over a large ZNMF with small blowing-suction velocity. An analysis of the flow around the wing-flap system as well as the turbulent structures of the wake are provided. In the best case, the studied ZNMF is able to mitigate the flow separation which leads to an important wake thinning down to 30% and an improvement of the lift-to-drag ratio up to 17.6%. From an energetic perspective, the ZNMF devices also appear really promising when the power saving due to drag reduction is much higher than the one supplied to the jet. Moreover, other interesting parameters such as the frequency and the velocity were also examined to obtain the optimal operating conditions of the ZNMF on the morphing high-lift system.

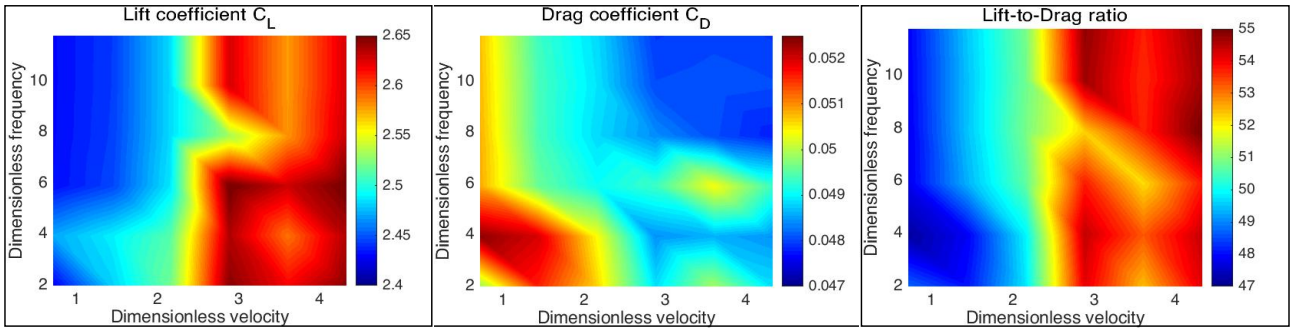

Figure 10: The lift, drag coefficient and the lift-to-drag ratio of the high-lift system with respect to variation of the dimensionless velocity and frequency.

ACKNOWLEDGEMENT

The results presented in this paper were obtained in the H2020 project SMS (funded by the European Union H2020 research and innovation framework programme under Grant Agreement 723402) and the CleanSky2 project AFC4TR (funded by the European Union H2020 programme under Grant Agreement 886718). This work was granted access to the HPC resources of [CINES/IDRIS/TGCC] under the allocation 2020-2021-2022-[A0102A11355] made by GENCI and HPC Strasbourg.

References

Donovan, J., Kral, L., and Cary, A. *Active flow control applied to an airfoil*. 1998. doi: 10.2514/6.1998-210.

Duvigneau, R. and Visonneau, M. Optimization of a synthetic jet actuator for aerodynamic stall control. *Computers & Fluids*, 35(6):624–638, 2006. doi: https://doi.org/10.1016/j.compfluid.2005.01.005.

Gilarranz, J., Traub, L., and Rediniotis, O. A new class of synthetic jet actuators—part II: Application to flow separation control. *Journal of Fluids Engineering-transactions of The Asme - J FLUID ENG*, 127, 2005. doi: 10.1115/1.1882393.

Hoarau, Y., Pena, D., Vos, J. B., Charbonier, D., Gehri, A., Braza, M., Deloze, T., and Laurendeau, E. *Recent Developments of the Navier Stokes Multi Block (NSMB) CFD solver*. 2016. doi: 10.2514/6.2016-2056.

Kim, S. H. and Kim, C. Separation control on naca23012 using synthetic jet. *Aerospace Science and Technology*, 13(4):172–182, 2009. doi: https://doi.org/10.1016/j.ast.2008.11.001.

Marouf, A., Yannick, B., Simiriotis, N., Tô, J.-B., Rouchon, J.-F., Hoarau, Y., and Braza, M. Numerical investigation of frequency-amplitude effects of dynamic morphing for a high-lift configuration at high Reynolds number. *International Journal of Numerical Methods for Heat and Fluid Flow*, 2019. doi: 10.1108/HFF-07-2019-0559.

Marouf, A., Chouippe, A., Vos, J. B., Charbonnier, D., Gehri, A., Braza, M., and Hoarau, Y. Unsteady cfd simulations for active flow control. *AIAA AVIATION 2021 Forum*, 2021. doi: 10.2514/6.2021-2854.

Marouf, A., Truong, H., Hoarau, Y., Gehri, A., Charbonnier, D., Vos, J. B., and Braza, M. Cfd simulations of active flow control devices applied on a cambered flap. *AIAA SCITECH 2022 Forum*, 2022. doi: 10.2514/6.2022-1545.

McCormick, D. *Boundary layer separation control with directed synthetic jets*. 2000. doi: 10.2514/6.2000-519.

Montazer, E., Mirzaei, M., Salami, E., Ward, T., Romli, F., and Kazi, S. Optimization of a synthetic jet actuator for flow control around an airfoil. *IOP Conference Series: Materials Science and Engineering*, 152:012023, 10 2016. doi: 10.1088/1757-899X/152/1/012023.

Seifert, A. and Pack, L. G. Oscillatory control of separation at high reynolds numbers. *AIAA Journal*, 37(9): 1062–1071, 1999. doi: 10.2514/2.834.

Tang, H., Salunkhe, P., Zheng, Y., Du, J., and Wu, Y. On the use of synthetic jet actuator arrays for active flow separation control. *Experimental Thermal and Fluid Science*, 57:1–10, 2014. ISSN 0894-1777. doi: https://doi.org/10.1016/j.expthermflusci.2014.03.015.

Tuck, A. and Soria, J. Active flow control over a NACA0015 airfoil using a ZNMF jet. In *The University of Sydney*, page 00178, 2004.

Welch, P. The use of fast fourier transform for the estimation of power spectra: A method based on time averaging over short, modified periodograms. *IEEE Transactions on Audio and Electroacoustics*, 15(2): 70–73, 1967. doi: 10.1109/TAU.1967.1161901.

You, D. and Moin, P. Active control of flow separation over an airfoil using synthetic jets. *Journal of Fluids and Structures*, 24(8):1349–1357, 2008. doi: https://doi.org/10.1016/j.jfluidstructs.2008.06.017.